

Full self-consistency versus quasiparticle self-consistency in diagrammatic approaches: Exactly solvable two-site Hubbard Model

A.L. Kutepov

Ames Laboratory USDOE, Ames, IA 50011

Self-consistent solutions of Hedin's diagrammatic theory equations (HE) for the two-site Hubbard Model (HM) have been studied. They have been found for three-point vertices of increasing complexity ($\Gamma = 1$ (GW approximation), Γ_1 from the first order perturbation theory, and exact vertex Γ_E). The comparison is being made when an additional quasiparticle (QP) approximation for the Green function is applied during the self-consistent iterative solving of HE and when QP approximation is not applied. The results obtained with the exact vertex are directly related to the presently open question - which approximation is more advantageous for future implementations - GW+DMFT or QPGW+DMFT. It is shown that in the regime of strong correlations only originally proposed GW+DMFT scheme is able to provide reliable results. Vertex corrections based on Perturbation Theory (PT) systematically improve the GW results when full self-consistency is applied. The application of the QP self-consistency combined with PT vertex corrections shows similar problems to the case when the exact vertex is applied combined with QP sc. The analysis of Ward Identity violation is performed for all studied in this work approximations and its relation to the general accuracy of the schemes used is provided.

PACS numbers: 71.10.Fd, 71.27.+a

I. INTRODUCTION

One of the challenges for the computational theorists working in the solid state electronic structure field is the robust implementation of the so called GW+DMFT method (combination of GW approximation (G- Green's function, W - screened interaction) and Dynamical Mean-Field Theory). The scheme was originally proposed by Sun and Kotliar¹ and in slightly different (but probably more commonly known) form by Biermann et al.² The basic idea of the approach is to separate all active space of the basis set into "weakly correlated" part for which GW approximation is supposed to work well and "strongly correlated" part for which one sums up many diagrams (to infinite order if one uses the non-perturbative DMFT solver as for example the Quantum Monte Carlo - QMC). In order for the method to be well defined, everything should be done till full self-consistency (sc), including the iterations of the GW part itself and also the "internal" iterations of DMFT part to ensure that the solution of the impurity problem reproduces the same G and W in strongly correlated subspace as the ones in the same subspace projected from the GW part.

Despite its obvious appeal GW+DMFT has made only slow progress during more than decade since its first appearance in the above mentioned papers. The reason was not just because scGW is quite demanding computationally but mostly because one has to satisfy the impurity sc condition not only for G (as in the LDA+DMFT method - a combination of Local Density Approximation in Density Functional Theory and DMFT) but also for the W, which seems to be not an easy task. To the best of my knowledge there were only "one-shot" type calculations for real materials³ where GW iterations were neglected altogether and DMFT self-consistency was imposed only

on G, whereas W was fixed at LDA level and correspondingly the U was considered as an external parameter (calculated in constrained random phase approximation - cRPA). Such an implementation, of course, is a definite step towards the full GW+DMFT scheme, but still one cannot say that there was the summation of all "correlated" graphs in it which would require that the W in GW part and W_{imp} in the impurity (DMFT) part were the same. Instead they were totally decoupled which makes it unclear of what kind of diagrams from DMFT part were actually added to GW part. Nevertheless, together with development of QMC solvers capable to handle dynamical interactions,^{4,5} the hope is growing that the full GW+DMFT scheme will eventually be implemented.

There are some subtleties about the GW part as well. In its full sc implementation the method is very time consuming which in part has prevented its applications for the real materials. But recently a very efficient implementation of it was published⁶ where the most computationally demanding parts (calculation of the polarizability P and the self energy Σ) are performed in real space and Matsubara's time. As a result, it became possible to successfully apply scGW to the actinides Pu and Am and (earlier) to simple sp-materials.⁷ However for the majority of solids, scGW produces worse spectra than fast "one-shot" GW and this is the other reason why scGW is not popular. The reason for the failure of scGW with spectra may be traced as an extremely non symmetrical "dressing" of the "initial" Green's function with self energy insertions of GW-only form in the course of self-consistency iterations and neglecting by vertex corrections.

The origin of the problem with the scGW method can also be formulated in terms of the absence of the Z-factor cancelation,⁸ which again happens because we neglect by the vertex corrections. To resolve this prob-

lem Kotani and Schilfsgaarde⁸ devised a beautiful trick of doing yet another approximation. They used quasi-particle (QP) part of Green's function G_{QP} (instead of full Green's function G calculated from Dyson's equation (DE)) to calculate P and Σ on every iteration till self-consistency. The trick is, that the errors from the above two approximations (using G_{QP} instead of full G and neglecting by vertex corrections) mostly cancel each other out and as a result the QPscGW (self-consistent quasi-particle GW) method usually gives much better spectra than full scGW. The important fact is that QPscGW not just slightly improves the one-shot GW description of sp-materials (which are good enough already in the one-shot GW), but often gives reasonable results for the materials with d- or f-electrons too,⁹ and the method doesn't rely on a particular starting point. It is totally self-consistent.

Quite naturally, the success of QPscGW with spectral properties (as compared to the full scGW) has ignited the ideas to formulate another approach - QPscGW+DMFT^{10,11}, where one supposedly adds DMFT corrections to P and Σ as in GW+DMFT but uses QPscGW for the "big" iterations in the "weakly correlated" part.

As it appears we have now two schemes proposed: GW+DMFT and QPGW+DMFT. In this work I am doing an attempt to "estimate" what to expect from the future implementation of the schemes. The analysis strongly depends on the "separability" of weakly and strongly correlated parts. I will assume here that they are perfectly separable and the correlations in the GW part are really weak. In this case, Z-factor in the GW part is close to 1, so that this part is equally well described in both the GW and the QPGW approximations. The difference correspondingly comes only from the DMFT part. For this part I assume that we are able to solve it exactly which means in particular that both sc conditions (for G and W) are satisfied. For GW+DMFT, it means $G = G_{imp}$, $W = W_{imp}$, and for QPGW+DMFT, it means $G_{QP} = G_{imp}$, $W_{QP} = W_{imp}$, where following the arguments of work [8] we have $G_{QP} \approx \frac{G}{Z}$. The exact solution of the impurity problem also means that corresponding self energies can be written in their exact diagrammatic forms: $\Sigma = -GTW$ and $\Sigma_{QP} = -G_{QP}\Gamma W_{QP}$ with Γ being the three-point vertex function which is included exactly. But following again the arguments in Ref.[8], it becomes clear that in QPGW+DMFT case, i.e. when we include exact vertex and continue to apply QP approximation for G , we will have a problem, because the factor $1/Z$ appears from the vertex and it doesn't cancel with the Z-factor in G as it happens in GW+DMFT. Basically it means the violation of Ward Identity (WI) in the QPGW+DMFT scheme. Thus, from this point of view, QPGW+DMFT is highly problematic and its difficulties should grow up when the correlation strength grows up, because the $1/Z$ -factor increases.

The above simple argument against using the QPGW+DMFT scheme for strongly correlated materials needs some numerical support and I will provide it

here using the exactly solvable two-site Hubbard model. For this model I calculate exactly the three-point vertex function and use it to calculate self-consistently the Green functions G and G_{QP} following two slightly different sc schemes (the scheme on the left side is basically the Hedin's sc equations¹² but with the 3-point vertex precalculated exactly)

$$\begin{aligned} P &= G\Gamma_{Exact}G & P_{QP} &= G_{QP}\Gamma_{Exact}G_{QP} \\ W &= U + UPW & W_{QP} &= U + UP_{QP}W_{QP} \\ \Sigma &= -G\Gamma_{Exact}W & \Sigma_{QP} &= -G_{QP}\Gamma_{Exact}W_{QP} \\ G &= G_0 + G_0\Sigma G & G_{QP} &= \frac{1}{Z} \frac{G_0}{1 - G_0\Sigma_{QP}}, \end{aligned} \quad (1)$$

where U is the bare interaction in the Hubbard model and G_0 is Green's function in Hartree approximation. In (1) for QP case I formally represented the quasiparticle approximation for G by simply dividing the full Green function from Dyson's equation by the Z-factor. This is for brevity. In fact I use the algorithm described in Ref.[6] to construct G_{QP} .

It is obvious that at self-consistency the scheme on the left side (I will call it GT_EW) is equivalent to the exact solution of GW+DMFT equations whereas the right hand scheme (I will call it $QPGT_EW$) is equivalent to the exact solution of the QPGW+DMFT equations. It is also obvious that the GT_EW scheme is exact by construction. I use it in this work to check the numerical accuracy of 3-point vertex evaluation. The $QPGT_EW$ scheme is approximate and below I will explore its accuracy in different regimes of correlation strength for the 2-site Hubbard model. Also I will directly relate the problems of the $QPGT_EW$ scheme with the degree of the WI violation.

Another goal of the present work was to explore the possibility of combining the GW and the QPGW methods with perturbative calculation of the 3-point vertex function. To this end I will use again the schemes similar to Eq.(1) but with Γ expanded to the first order in W (Γ_1) instead of exact Γ_E . I also will show how the two corresponding perturbation theory based schemes (GT_1W and $QPGT_1W$) behave in the different regimes of parameters of the Hubbard model.

This paper begins with the formal presentation of the two-site Hubbard model and the formulae used in the calculations (Section II). In Section III the results are presented and discussed. Finally in Section IV the conclusions are given and the future plans are outlined.

II. TWO-SITE HUBBARD MODEL

The Hamiltonian of two-site Hubbard model as it is used in this work is the following:

$$H = -t \sum_{i \neq j, \sigma} c_{i\sigma}^\dagger c_{j\sigma} + \frac{U}{2} \sum_i \sum_{\sigma\sigma'} c_{i\sigma}^\dagger c_{i\sigma'}^\dagger c_{i\sigma'} c_{i\sigma}, \quad (2)$$

where t and U are the standard parameters of the Hubbard model, c and c^+ are the destruction and creation operators correspondingly, indexes i and j belong to the sites (1 or 2), and σ, σ' are the spin indexes.

In this section, all equations which are used in the analysis of the 2-site Hubbard model are collected for references. First I provide the energies and eigen vectors of the exact many-body states of the model for different occupancies. Then, the exact expressions for Green function and density-density correlation function are given. From them the exact self energy, polarizability, dielectric function, and screened interaction can be calculated using standard formulae. Next, two subsections provide the formulae for the exact 3-point vertex function and how it is used to evaluate the corrections to the polarizability and to the self energy in sc scheme (1). Perturbation theory based equations for the 3-point vertex function are given next. Then I provide full and reduced (long-wave and long-wave+static limits) expressions for the Ward Identity which are used later in this paper. Finally the formulae relevant to the evaluation of current three-point vertex function are given. For brevity, the derivations of the formulae are not provided, or only sketch of derivation is given. In this work, the finite temperature framework is used so that in all equations below the time-frequency arguments are Matsubara's time (τ) and Matsubara's frequencies (ω for fermion frequency and ν for boson frequency).

A. Many-body states

In order to represent the many-body states of the model it is convenient to introduce basis vectors $|abcd\rangle$ where all entries are equal to 0 or 1 in accordance with the occupancies of corresponding one-electron states. In this work first two one-electron occupancies (a and b) correspond to spin-up and spin-down one-electron states of the first site, and the third and fourth (c and d) correspond to the second site. Many-body energies and states below have two indexes: the upper one corresponds to the full occupancy (0,1,2,3, or 4) of the system, and the lower one distinguishes the states within the same occupancy.

For the full occupancy N equal zero, we have correspondingly:

$$E_1^0 = 0; \Psi_1^0 = |0000\rangle, \quad (3)$$

for N=1

$$\begin{aligned} E_1^1 &= -t; \Psi_1^1 = \frac{1}{\sqrt{2}}(|1000\rangle + |0010\rangle) \\ E_2^1 &= -t; \Psi_2^1 = \frac{1}{\sqrt{2}}(|0100\rangle + |0001\rangle) \\ E_3^1 &= t; \Psi_3^1 = \frac{1}{\sqrt{2}}(|1000\rangle - |0010\rangle) \\ E_4^1 &= t; \Psi_4^1 = \frac{1}{\sqrt{2}}(|0100\rangle - |0001\rangle), \end{aligned} \quad (4)$$

for N=2

$$\begin{aligned} E_1^2 &= \frac{U-c}{2}; \Psi_1^2 = 4t \frac{|1001\rangle - |0110\rangle}{\sqrt{a(c-U)}} + \frac{|1100\rangle + |0011\rangle}{a} \\ E_2^2 &= 0; \Psi_2^2 = |1010\rangle \\ E_3^2 &= 0; \Psi_3^2 = |0101\rangle \\ E_4^2 &= 0; \Psi_4^2 = \frac{1}{\sqrt{2}}(|1001\rangle + |0110\rangle) \\ E_5^2 &= U; \Psi_5^2 = \frac{1}{\sqrt{2}}(|1100\rangle - |0011\rangle) \\ E_6^2 &= \frac{U+c}{2}; \Psi_6^2 = 4t \frac{|1001\rangle - |0110\rangle}{\sqrt{b(c+U)}} - \frac{|1100\rangle + |0011\rangle}{b}, \end{aligned} \quad (5)$$

with $a = \sqrt{2 + \frac{32t^2}{(U-c)^2}}$, $b = \sqrt{2 + \frac{32t^2}{(U+c)^2}}$, and $c = \sqrt{16t^2 + U^2}$.

For N=3

$$\begin{aligned} E_1^3 &= U - t; \Psi_1^3 = \frac{1}{\sqrt{2}}(|1011\rangle - |1110\rangle) \\ E_2^3 &= U - t; \Psi_2^3 = \frac{1}{\sqrt{2}}(|0111\rangle - |1101\rangle) \\ E_3^3 &= U + t; \Psi_3^3 = \frac{1}{\sqrt{2}}(|1011\rangle + |1110\rangle) \\ E_4^3 &= U + t; \Psi_4^3 = \frac{1}{\sqrt{2}}(|0111\rangle + |1101\rangle), \end{aligned} \quad (6)$$

and for N=4

$$E_1^4 = 2U; \Psi_1^4 = |1111\rangle. \quad (7)$$

B. The Partition function, Green's function and self energy

For convenience, first I introduce "shifted" many-body energies $E_n'^N = E_n^N - \mu N$, with μ being the chemical potential. Then I renormalize them, defying the minimal E'_{min} among them and subtracting it $E_n''^N = E_n'^N - E'_{min}$. This also factorizes the partition function:

$$\begin{aligned} Z(\mu) &= \sum_{nN} e^{-\beta E_n'^N} = e^{-\beta E'_{min}} \sum_{nN} e^{-\beta E_n''^N} \\ &= e^{-\beta E'_{min}} Z'(\mu), \end{aligned} \quad (8)$$

where β is the inverse temperature.

It is clear that now in every Gibbs average one can use $E''; Z'$ instead of $E'; Z$ which is numerically more stable (big numbers have been subtracted).

For exact Green's function, one obtains through the standard spectral decomposition:

$$\begin{aligned} G_{ij}^\sigma(\omega) &= \frac{1}{Z'} \sum_N \sum_{n \in N} \sum_{m \in N+1} \frac{e^{-\beta E_m''^{N+1}} + e^{-\beta E_n''^N}}{i\omega - E_{mN+1}'' + E_{nN}''} \\ &\quad \times \langle \Psi_n^N | c_{i\sigma} | \Psi_m^{N+1} \rangle \langle \Psi_m^{N+1} | c_{j\sigma}^\dagger | \Psi_n^N \rangle. \end{aligned} \quad (9)$$

The exact self energy is obtained by inversion of the Dyson's equation:

$$\Sigma_{ij}^\sigma(\omega) = G_{0,ij}^{-1\sigma}(\omega) - G_{ij}^{-1\sigma}(\omega), \quad (10)$$

where Green's function in Hartree approximation $G_{0,ij}^{-1\sigma}(\omega) = (i\omega + \mu - U\rho_i)\delta_{ij} + t(1 - \delta_{ij})$ is used (ρ_i is the occupancy ("density") of the site i).

C. Response function, polarizability, dielectric function, and W

The exact two-point density-density correlation function is also obtained through the spectral decomposition

$$\chi_{ij}^{dd}(\nu) = \frac{1}{Z'} \sum_N \sum_{n \in N} \sum_{m \in N} \frac{e^{-\beta E_m''N} - e^{-\beta E_n''N}}{i\nu + E_{nN}'' - E_{mN}''} \times \langle \Psi_n^N | \hat{\rho}_i | \Psi_m^N \rangle \langle \Psi_m^N | \hat{\rho}_j | \Psi_n^N \rangle, \quad (11)$$

with density operator $\hat{\rho}_i = \sum_{\sigma} c_{i\sigma}^{\dagger} c_{i\sigma}$. It is convenient to define also the density-density response function

$$R_{ij}^{dd}(\nu) = \beta \delta_{\nu 0} \rho_i \rho_j - \chi_{ij}^{dd}(\nu). \quad (12)$$

After that one can find the density-density dielectric function

$$\epsilon_{ij}^{-1dd}(\nu) = \delta_{ij} + U R_{ij}^{dd}(\nu), \quad (13)$$

the density-density polarizability

$$P_{ij}^{dd}(\nu) = \sum_k R_{ik}^{dd}(\nu) \epsilon_{kj}^{dd}(\nu), \quad (14)$$

and the screened interaction

$$W_{ij}(\nu) = U \delta_{ij} + U^2 R_{ij}^{dd}(\nu). \quad (15)$$

The response function, the dielectric function, the polarizability, and the screened interaction calculated using the formulae (12)-(15) from the exact correlation function are by construction exact and can be compared with the corresponding quantities obtained using the PT.

D. Exact 3-point vertex function in density channel

To find the exact 3-point density vertex function I first calculate the following three-point correlation function: $\chi_{ijk}^{\sigma,d}(\tau; \tau') = \langle c_{i\sigma}(\tau) c_{j\sigma}^{\dagger}(\tau') \hat{\rho}_k(0) \rangle$ with τ, τ' being Matsubara's times and 'd' meaning 'density'. In the site-frequency domain its spectral decomposition reads as the following:

$$\begin{aligned} \chi_{ijk}^{\sigma,d}(\omega; \nu) = \frac{1}{Z'} \sum_N \{ & - \sum_{p \in N} \sum_{n \in N+1} \frac{\langle \Psi_n^{N+1} | c_{j\sigma}^{\dagger} | \Psi_p^N \rangle}{i(\omega - \nu) + E_p''N - E_n''N+1} \sum_{m \in N+1} \langle \Psi_p^N | c_{i\sigma} | \Psi_m^{N+1} \rangle \langle \Psi_m^{N+1} | \hat{\rho}_k | \Psi_n^{N+1} \rangle \frac{e^{-\beta E_m''N+1} - e^{-\beta E_n''N+1}}{i\nu + E_n''N+1 - E_m''N+1} \\ & + \sum_{p \in N+1} \sum_{m \in N} \frac{\langle \Psi_p^{N+1} | c_{j\sigma}^{\dagger} | \Psi_m^N \rangle}{-i(\omega - \nu) + E_p''N+1 - E_m''N} \sum_{n \in N} \langle \Psi_n^N | c_{i\sigma} | \Psi_p^{N+1} \rangle \langle \Psi_m^N | \hat{\rho}_k | \Psi_n^N \rangle \frac{e^{-\beta E_m''N} - e^{-\beta E_n''N}}{i\nu + E_n''N - E_m''N} \\ & + \sum_{p \in N} \sum_{n \in N+1} \frac{\langle \Psi_n^{N+1} | c_{j\sigma}^{\dagger} | \Psi_p^N \rangle}{i(\omega - \nu) + E_p''N - E_n''N+1} \sum_{m \in N+1} \langle \Psi_p^N | c_{i\sigma} | \Psi_m^{N+1} \rangle \langle \Psi_m^{N+1} | \hat{\rho}_k | \Psi_n^{N+1} \rangle \frac{e^{-\beta E_m''N+1} + e^{-\beta E_p''N}}{i\omega + E_p''N - E_m''N+1} \\ & + \sum_{p \in N+1} \sum_{m \in N} \frac{\langle \Psi_p^{N+1} | c_{j\sigma}^{\dagger} | \Psi_m^N \rangle}{-i(\omega - \nu) + E_p''N+1 - E_m''N} \sum_{n \in N} \langle \Psi_n^N | c_{i\sigma} | \Psi_p^{N+1} \rangle \langle \Psi_m^N | \hat{\rho}_k | \Psi_n^N \rangle \frac{e^{-\beta E_p''N+1} + e^{-\beta E_n''N}}{i\omega + E_n''N - E_p''N+1} \}. \end{aligned} \quad (16)$$

After that the three-point density response function is calculated

$$R_{ijk}^{\sigma,d}(\omega; \nu) = \frac{\delta G_{ij}^{\sigma}(\omega)}{\delta \phi_k(\nu)} = \beta \delta_{\nu 0} G_{ij}^{\sigma}(\omega) \rho_k + \chi_{ijk}^{\sigma,d}(\omega; \nu), \quad (17)$$

where I have indicated that the three-point response function is defined as the functional derivative of Green's function with respect to the external perturbing field

$\phi_k(\nu)$. The "screened" 3-point density vertex function $\gamma_{ijk}^{\sigma,d}(\omega; \nu)$ is defined as the functional derivative of the inverse Green's function with respect to the external perturbing field $\phi_k(\nu)$ and correspondingly can be related to the above defined 3-point response function

G. Ward Identities

In order to write down the Ward Identities one needs to specify the current operator. It is convenient to introduce it through the substitution for the kinetic part of the Hamiltonian

$$H' = -t \sum_{i\sigma} c_{i\sigma}^+ e^{i(A_i - A_i)} c_{i\sigma} + \frac{U}{2} \sum_i \sum_{\sigma\sigma'} c_{i\sigma}^+ c_{i\sigma'}^+ c_{i\sigma'} c_{i\sigma}, \quad (24)$$

where A_i is the vector potential and the following convention for the sites was adopted: $\hat{1} = 2; \hat{2} = 1$. With the above definition the current operator for the model reads as the following

$$\hat{J}_i = -\frac{\delta H'}{\delta A_i} = it \sum_{\sigma} \{c_{i\sigma}^+ c_{i\sigma} - c_{i\sigma}^+ c_{i\sigma}\}, \quad (25)$$

with $\hat{J}_{\hat{i}} = -\hat{J}_i$. From the equation of motion for the density operator one calculates

$$\frac{\partial \hat{\rho}_i}{\partial \tau} = -i \hat{J}_i, \quad (26)$$

which is the continuity equation for the model. Relating the "screened" 3-point current vertex function with the corresponding 3-point response function (similarly to the density case and in the space-time coordinates for brevity; 'c' goes for 'current')

$$G^\sigma(14) \gamma^{\sigma,c}(453) G^\sigma(52) = G^\sigma(12) J(3) + \langle c_\sigma(1) c_\sigma^+(2) \hat{J}(3) \rangle, \quad (27)$$

one explicitly calculates the time derivatives and using also the continuity equation (26) one obtains

$$\begin{aligned} G^\sigma(14) \left\{ \frac{\partial}{\partial \tau_3} \gamma^{\sigma,d}(453) + i \gamma^{\sigma,c}(453) \right\} G^\sigma(52) \\ = \frac{\partial}{\partial \tau_3} \langle c_\sigma(1) c_\sigma^+(2) \hat{\rho}(3) \rangle + i \langle c_\sigma(1) c_\sigma^+(2) \hat{J}(3) \rangle \\ = G^\sigma(12) \left\{ \delta(13) - \delta(23) \right\}, \end{aligned} \quad (28)$$

which is equivalent to

$$\frac{\partial}{\partial \tau_3} \gamma^{\sigma,d}(123) + i \gamma^{\sigma,c}(123) = G^{-1\sigma}(12) \left\{ \delta(23) - \delta(13) \right\}. \quad (29)$$

In the site-frequency representation (29) reads as the following

$$\begin{aligned} i \left\{ \nu \gamma_{ijk}^{\sigma,d}(\omega; \nu) + \gamma_{ijk}^{\sigma,c}(\omega; \nu) \right\} \\ = G_{ij}^{-1\sigma}(\omega) \delta_{jk} - G_{ij}^{-1\sigma}(\omega - \nu) \delta_{ik}. \end{aligned} \quad (30)$$

$$\begin{aligned} \gamma_{ijk}^{\sigma,d}(\omega; \nu) &= -\frac{\delta G_{ij}^{-1\sigma}(\omega)}{\delta \phi_k(\nu)} \\ &= \sum_{lt} G_{il}^{-1\sigma}(\omega) R_{ltk}^{\sigma,d}(\omega; \nu) G_{tj}^{-1\sigma}(\omega - \nu). \end{aligned} \quad (18)$$

Finally the three-point vertex function entering the Eq.(1) ("bare" three-point vertex) is defined as the functional derivative of the inverse Green's function with respect to the total field $\Phi_k(\nu)$ (perturbing external plus induced internal) and is related to the "screened" vertex through the density-density dielectric matrix (this equation is the density-density part of the more general equation (41))

$$\begin{aligned} \Gamma_{ijk}^{\sigma,d}(\omega; \nu) &= -\frac{\delta G_{ij}^{-1\sigma}(\omega)}{\delta \Phi_k(\nu)} \\ &= \sum_l \gamma_{ijl}^{\sigma,d}(\omega; \nu) \epsilon_{lk}^{dd}(\nu). \end{aligned} \quad (19)$$

E. Vertex corrected polarizability and self energy

The vertex-corrected density-density polarizability and the self energy entering the equations (1) are calculated as the following

$$P_{ij}^{dd}(\nu) = \frac{1}{\beta} \sum_{\omega} \sum_{\sigma} \sum_{kl} G_{ik}^{\sigma}(\omega) \Gamma_{klj}^{\sigma,d}(\omega; \nu) G_{li}^{\sigma}(\omega - \nu), \quad (20)$$

and

$$\Sigma_{ij}^{\sigma}(\omega) = -\frac{1}{\beta} \sum_{\nu} \sum_{kl} G_{ik}^{\sigma}(\omega + \nu) \Gamma_{klj}^{\sigma,d}(\omega + \nu; \nu) W_{li}(\nu). \quad (21)$$

The formulae (20) and (21) are used also when the three-point vertex is obtained within the perturbation theory.

F. 3-point vertex function from Perturbation Theory in density channel

The first order (in W) term of the perturbation theory for the three-point density vertex function is

$$\Gamma_{ijk}^{\sigma,d}(\tau; \tau') = -W_{ji}(\tau' - \tau) G_{ik}^{\sigma}(\tau) G_{kj}^{\sigma}(-\tau'). \quad (22)$$

In the frequency representation it can be conveniently evaluated as the following

$$\Gamma_{ijk}^{\sigma,d}(\omega; \nu) = -\int d\tau W_{ji}(\tau) \frac{1}{\beta} \sum_{\omega} e^{-i\omega\tau} G_{ik}^{\sigma}(\omega) G_{kj}^{\sigma}(\omega - \nu). \quad (23)$$

The equation (30) can be simplified by removing the Hartree-Fock contribution on the both sides of it. For the vertices, one obtains in the Hartree-Fock approximation

$$\gamma_{ijk}^{\sigma,d}(\omega; \nu) = \delta_{ik}\delta_{jk}, \quad (31)$$

and

$$\gamma_{ijk}^{\sigma,c}(\omega; \nu) = it\{\delta_{ik} - \delta_{jk}\}. \quad (32)$$

For the schemes with full sc (without the QP approximation) the removing of the Hartree-Fock contribution also on the right side of (30) through Dyson's equation gives

$$\begin{aligned} i\{\nu\Delta\gamma_{ijk}^{\sigma,d}(\omega; \nu) + \Delta\gamma_{ijk}^{\sigma,c}(\omega; \nu)\} \\ = \Sigma_{ij}^{c,\sigma}(\omega - \nu)\delta_{ik} - \Sigma_{ij}^{c,\sigma}(\omega)\delta_{jk}, \end{aligned} \quad (33)$$

where $\Delta\gamma$ means the "screened" vertex part beyond the Hartree-Fock approximation, and the Σ^c is the correlation (frequency dependent) part of the self energy. For the QP-based schemes the Dyson equation is not satisfied and instead of (33) one has

$$\begin{aligned} i\{\nu\Delta\gamma_{ijk}^{\sigma,d}(\omega; \nu) + \Delta\gamma_{ijk}^{\sigma,c}(\omega; \nu)\} \\ = \{H_{ij}^{HF} - H_{ij}^{QP}\}[\delta_{ik} - \delta_{jk}], \end{aligned} \quad (34)$$

where the static effective Hamiltonians H_{ij}^{HF} and H_{ij}^{QP} (correspondingly in the Hartree-Fock and in the QP approximation) were introduced:

$$H_{ij}^{HF} = -t(1 - \delta_{ij}) + \delta_{ij}(V_i^H + \Sigma_i^x), \quad (35)$$

with V_i^H and Σ_i^x being the Hartree potential and the exchange part of the self energy correspondingly, and

$$H_{ij}^{QP} = \mu[\delta_{ij} - Z_{ij}] + \sum_{kl} Z_{ik}^{1/2}[H_{kl}^{HF} + \Sigma_{kl}^c(0)]Z_{lj}^{1/2}, \quad (36)$$

where Z_{ij} is the renormalization factor, and the $\Sigma_{kl}^c(0)$ stands for the correlation part of the self energy at zero frequency. When the effect of correlations is neglected the renormalization factor becomes equal to 1, and the correlation part of the self energy becomes zero, which means that in this case $H^{QP} = H^{HF}$.

The equations (33) and (34) are used in this work to evaluate the deviations from the full Ward Identity for different approximate methods. I also use two reduced forms of the WI in the present study: the long-wave limit and the long-wave+static limit of the WI. The long-wave limit of the WI for the two-site Hubbard model consists in the summation over the index k in the equations (33) and (34) which correspondingly become (the current vertex disappears after the summation)

$$i\nu \sum_k \Delta\gamma_{ijk}^{\sigma,d}(\omega; \nu) = \Sigma_{ij}^{c,\sigma}(\omega - \nu) - \Sigma_{ij}^{c,\sigma}(\omega), \quad (37)$$

and

$$i\nu \sum_k \Delta\gamma_{ijk}^{\sigma,d}(\omega; \nu) = 0. \quad (38)$$

From (38) one can see that in order to satisfy the long-wave limit of the WI in the QP-based approximations one has to neglect by vertex corrections altogether.

The long-wave+static limit of the WI consists in taking the limit ($\nu \rightarrow 0$) in the equations (37) and (38):

$$\sum_k \Delta\gamma_{ijk}^{\sigma,d}(\omega; \nu = 0) = \lim_{\nu \rightarrow 0} \frac{\Sigma_{ij}^{c,\sigma}(\omega - \nu) - \Sigma_{ij}^{c,\sigma}(\omega)}{i\nu}, \quad (39)$$

and

$$\sum_k \Delta\gamma_{ijk}^{\sigma,d}(\omega; \nu = 0) = 0. \quad (40)$$

The arguments supporting the quasiparticle approximation in Ref.[8] are based on the long wave limit of the Ward Identity. It is clear from the above consideration that in the QPGW approximation (without the vertex corrections) the corresponding limit of the WI is satisfied exactly.

H. 3-point current vertex function

In order to apply the full WI one needs the "screened" current vertex function $\gamma_{ijk}^{\sigma,c}(\omega; \nu)$. In this work both the exact and the PT-based vertex functions are used. The exact one is evaluated following the formulae (16)-(18) with the replacement ($\hat{\rho} \rightarrow \hat{J}$) in the Eq.(16). The PT-based vertices are calculated following the scheme outlined below.

The "bare" vertex functions are related to the "screened" ones through the full (density-current) dielectric function via the following equation which is the generalization of Eq.(19)

$$\gamma_{ijk}^{\sigma,I}(\omega; \nu) = \sum_J \sum_l \Gamma_{ijl}^{\sigma,J}(\omega; \nu) \epsilon_{lk}^{-1JI}(\nu), \quad (41)$$

where both I and J now run over the indices d (density) and c (current). The non-perturbed Hamiltonian has no vector potentials so that the full dielectric matrix has the form (considering the first index as the density, and the second as the current)

$$\epsilon = \begin{pmatrix} \epsilon^{dd} & \epsilon^{dc} \\ 0 & 1 \end{pmatrix}, \quad (42)$$

and correspondingly its inverse

$$\epsilon^{-1} = \begin{pmatrix} \epsilon^{-1dd} & -\epsilon^{-1dd}\epsilon^{dc} \\ 0 & 1 \end{pmatrix}. \quad (43)$$

Thus, the bare current vertex can be evaluated as the following

$$\begin{aligned} \gamma_{ijk}^{\sigma,c}(\omega; \nu) &= \Gamma_{ijl}^{\sigma,c}(\omega; \nu) \\ &- \sum_{lm} \Gamma_{ijl}^{\sigma,d}(\omega; \nu) \epsilon_{lm}^{-1dd}(\nu) \epsilon_{mk}^{dc}(\nu). \end{aligned} \quad (44)$$

The subtraction of the Hartree-Fock contribution (32) leaves us with the expression

$$\begin{aligned} \Delta\gamma_{ijk}^{\sigma,c}(\omega; \nu) &= \Delta\Gamma_{ijl}^{\sigma,c}(\omega; \nu) \\ &- \sum_{lm} [\delta_{il}\delta_{jl} + \Delta\Gamma_{ijl}^{\sigma,d}(\omega; \nu)] \epsilon_{lm}^{-1dd}(\nu) \epsilon_{mk}^{dc}(\nu). \end{aligned} \quad (45)$$

In the above expression the missing components are the non-trivial part of the current vertex $\Delta\Gamma_{ijl}^{\sigma,c}(\omega; \nu)$ and the density-current dielectric matrix $\epsilon_{mk}^{dc}(\nu)$. The first one is evaluated similar to the equation (23) for the density vertex:

$$\begin{aligned} \Delta\Gamma_{ijk}^{\sigma,c}(\omega; \nu) &= -it \int d\tau W_{ji}(\tau) \frac{1}{\beta} \sum_{\omega} e^{-i\omega\tau} \\ &\times \left\{ G_{ik}^{\sigma}(\omega) G_{kj}^{\sigma}(\omega - \nu) - G_{ik}^{\sigma}(\omega) G_{kj}^{\sigma}(\omega - \nu) \right\}. \end{aligned} \quad (46)$$

The second one is defined by the density-current polarizability P^{dc}

$$\epsilon_{ij}^{dc}(\nu) = -UP_{ij}^{dc}(\nu), \quad (47)$$

which in its turn is evaluated using the current vertex (46):

$$\begin{aligned} P_{ij}^{dc}(\nu) &= it \int d\tau e^{i\nu\tau} \sum_{\sigma} \left\{ G_{ij}^{\sigma}(\tau) G_{ji}^{\sigma}(-\tau) - G_{ij}^{\sigma}(\tau) G_{ji}^{\sigma}(-\tau) \right\} \\ &+ \frac{1}{\beta} \sum_{\omega} \sum_{\sigma} \sum_{kl} G_{ik}^{\sigma}(\omega) \Delta\Gamma_{klj}^{\sigma,c}(\omega; \nu) G_{li}^{\sigma}(\omega - \nu). \end{aligned} \quad (48)$$

I. Internal energy

The exact internal energy is evaluated directly as the average value of the Hamiltonian. In the spectral representation it reads

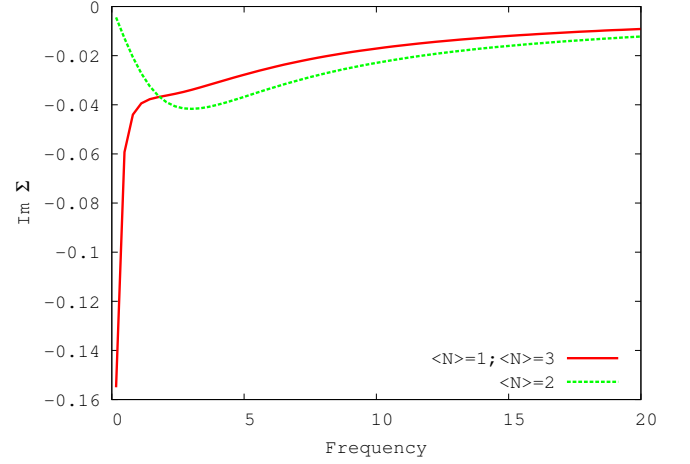


FIG. 1: (Color online) Imaginary part of the on-site self energy as a function of frequency for different average occupancies for $U=1$.

$$E = \frac{1}{Z'} \sum_{nN} E_n'' e^{-\beta E_n''}. \quad (49)$$

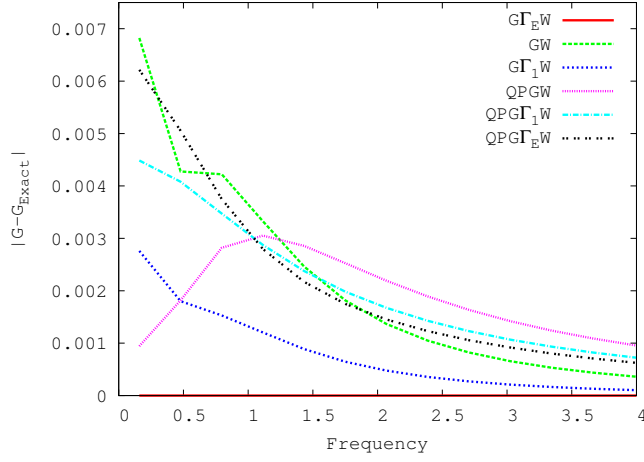
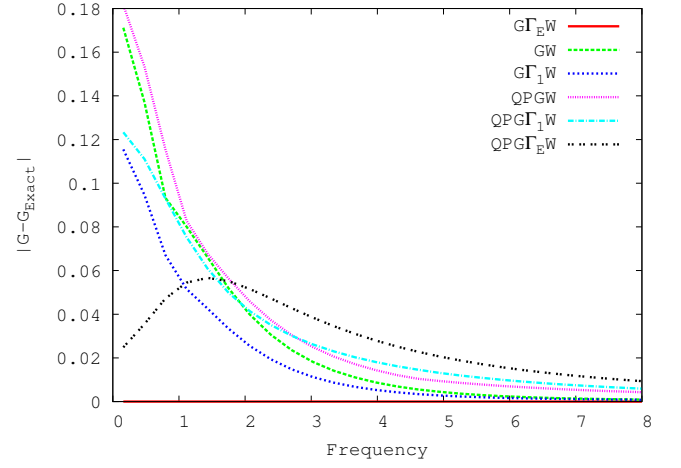
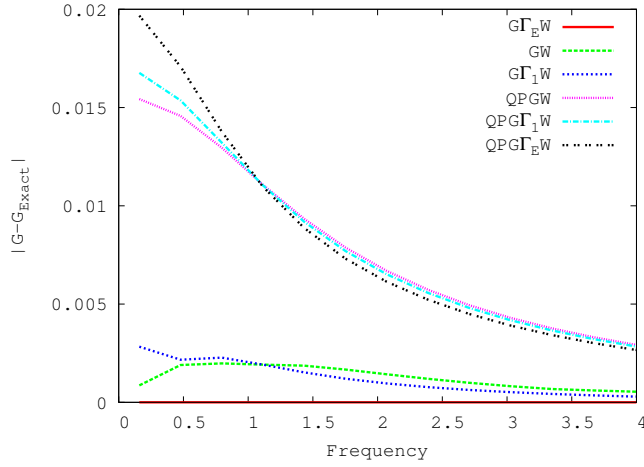
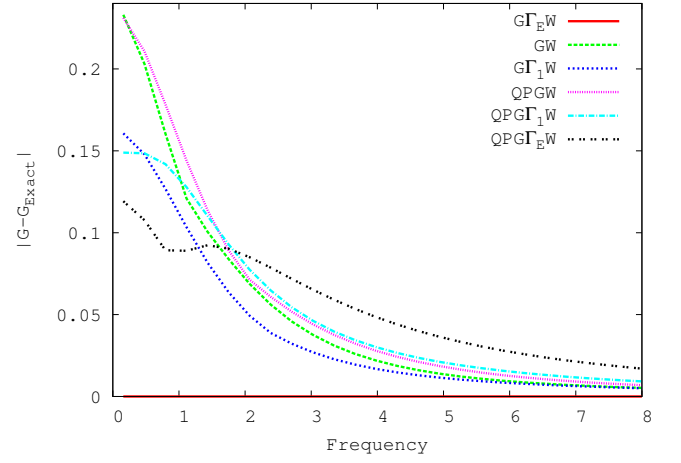
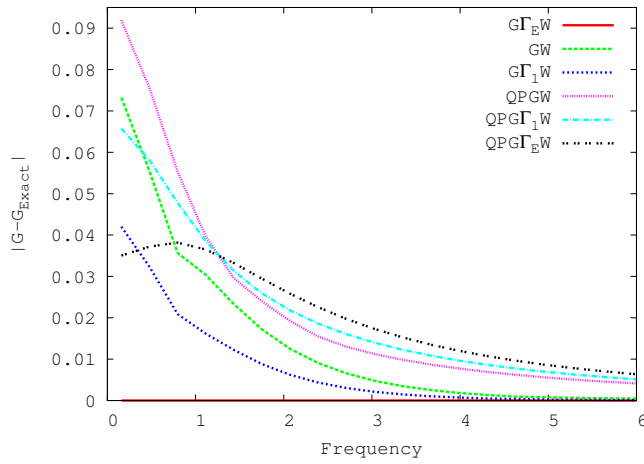
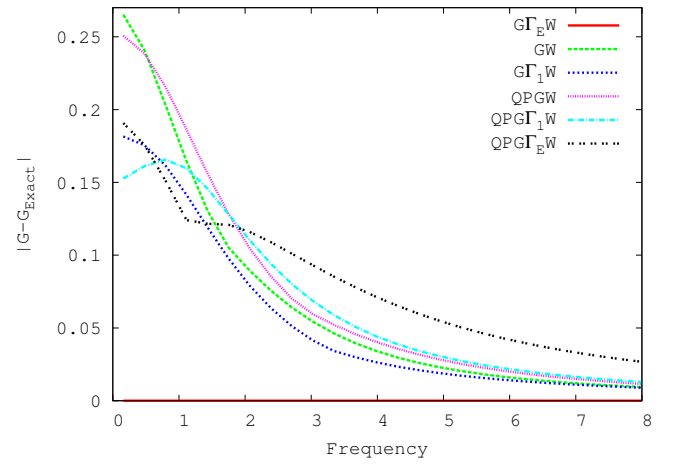
To evaluate the internal energy in the perturbation theory based methods the following formula is used

$$\begin{aligned} E &= t \sum_{i \neq j, \sigma} G_{ji}^{\sigma}(\tau = \beta) + \frac{U}{2} \sum_i \sum_{\sigma\sigma'} \rho_{i\sigma} \rho_{i\sigma'} \\ &- \frac{1}{2} \sum_i \sum_{\sigma} \Sigma_{ii}^{x,\sigma} G_{ii}^{\sigma}(\tau = \beta) \\ &+ \frac{1}{2\beta} \sum_{i\sigma} \sum_{\omega} \Sigma_{ij}^{c,\sigma}(\omega) G_{ji}^{\sigma}(\omega), \end{aligned} \quad (50)$$

which is based on the Galitskii-Migdal expression for the exchange-correlation energy.

III. RESULTS

The two-site Hubbard model is studied here with the value of parameter t fixed and equal to 1. The temperature was also fixed at $T=0.05t$. Thus, only the parameter U was changing. The half-filling ($\langle N \rangle = 2$) case has been considered. Such a choice for the occupancy has been guided mostly by the fact that when one steps aside from the half-filling the correlations in the model quickly become unmanageable for the QP-based approaches. It is seen in the Fig.1 where the imaginary part of the on-site self energy is plotted as a function of Matsubara's frequency for the average occupancies 1, 2, and 3.

FIG. 2: (Color online) Errors in Green's function for $U=0.5$.FIG. 5: (Color online) Errors in Green's function for $U=3$.FIG. 3: (Color online) Errors in Green's function for $U=1$.FIG. 6: (Color online) Errors in Green's function for $U=4$.FIG. 4: (Color online) Errors in Green's function for $U=2$.FIG. 7: (Color online) Errors in Green's function for $U=5$.

The strong downturn in the function for the occupancies 1 and 3 at the small frequencies makes the linearization in the self energy pertinent to the QP approximations highly inaccurate. At the half filling however, the model shows slow increasing in the correlation strength with the increasing of U and, correspondingly, is convenient for the comparative studies. The calculations have been performed for different values of U which were increased till the methods based on the QP approximation began to fail seriously.

I compare the exact results with the results obtained with the GW, the Γ_1 W, the Γ_E W, the QPGW, $\text{QPG}\Gamma_1$ W, and the $\text{QPG}\Gamma_E$ W methods, where Γ_1 and Γ_E stand for the first order (in W) 3-point vertex and the exact 3-point vertex correspondingly. At the full self-consistency Γ_E W reproduces the exact results, so this approach was used basically only as a mean to adjust (by comparing with the exact result) the calculational parameters (such as the number of Matsubara's frequencies included in the internal summations and the density of mesh on the interval $[0 : \beta]$ for the τ -integrations. In addition to the Green function which serves in this work as basic representation quantity for the comparisons, the analysis of the Ward Identities fulfillment has been performed and was used as an indicator of the accuracy of the approximations. Besides, the internal energy has been evaluated and its accuracy was related to the errors in the calculated G and to the deviations from the Ward Identities.

In the figures 2-7 the absolute error in the calculated Green's function is shown as a function of the Matsubara's frequency for the different values of U . The comparison is being made between the exact result and the results obtained with the approximate methods. The internal energy as a function of U is presented in the Fig.8. The figure 9 shows the relative violation of the full WI (Eqs.33 and 34) in different approximate methods as a function of U . The following form of the average deviation from the identity has been used

$$\frac{\sum_{\omega, \nu} \sum_{ijk} \left\| (LHS)_{ijk}(\omega; \nu) - (RHS)_{ijk}(\omega; \nu) \right\|}{\sum_{\omega, \nu} \sum_{ijk} 1}, \quad (51)$$

where (LHS) and (RHS) are the left- and the right-hand sides in (33,34) correspondingly. The 3-point vertex pertinent to the specific approximation (i.e. for instance the vertex $\Delta\gamma$ is zero in the GW and the QPGW) was used to evaluate the deviation from the WI in all approximate schemes, and the exact vertex was used in Γ_E W and $\text{QPG}\Gamma_E$ W. The summations over the frequencies ω and ν in (51) were performed for $|\omega| < 20$ and $0 \leq \nu < 20$.

The figure 10 shows the similar plot obtained with the long-wave limit of the WI (37,38). The formula analogous to (51) has been used but without the k -summation. Finally in the figure 11 the deviation from the long-wave+static limit of the WI (39,40) is shown. In this case, the summation over ν has not been included.

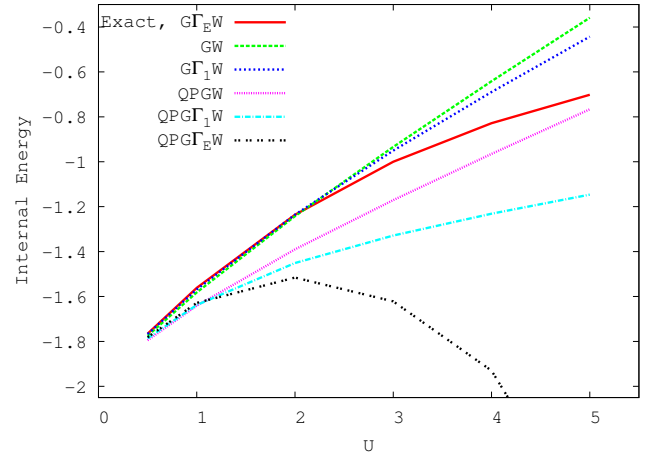


FIG. 8: (Color online) Internal energy as a function of U parameter.

One can do a few observations from the results presented.

Most important for the present work is an observation following from the errors in Green's function, that the $\text{QPG}\Gamma_E$ W method doesn't show any noticeable improvement as compared to the other approximate methods studied. Opposite to that - with U increasing it quickly becomes the worst of the methods considered (especially for the higher frequencies). The observation perfectly correlates with the results obtained for the internal energy and for the Ward Identities (especially with the results for the full WI). It means that putting the exact vertex together with the QP self-consistency is not compatible.

Grouping the methods based on the QP-approximation in one group and the rest of the methods in another (they satisfy the DE), one can do another conclusion.

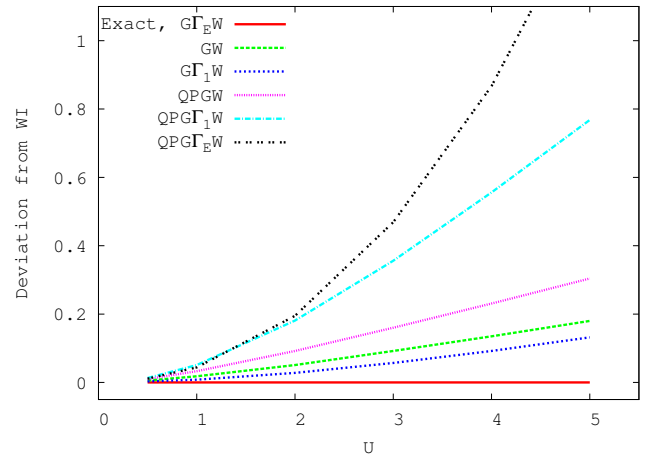


FIG. 9: (Color online) Full Ward Identity average violation as a function of U parameter.

Namely for the frequencies larger than approximately 1.5 the QP group has considerably larger errors in G than the group with the full self-consistency. This again correlates strongly with the internal energy graph and with the full WI.

Further, in the methods satisfying the Dyson equation the increasing in the accuracy of the vertex ($1 \rightarrow \Gamma_1 \rightarrow \Gamma_E$) consistently improves the accuracy of G , finally making it exact when the exact vertex is being applied. Naturally, the same tendency can be noticed looking at the internal energy graph and at all WI graphs.

Opposite to that, in the QP-based methods the situation is more complicated. At lowest U (0.5 and 1) the QPGW is the best and the QPG Γ_E W is the worst at low frequencies with the reversed tendency at high frequencies. For U equal 2, 3, and 4 one can notice that now the QPG Γ_E W is the best and the QPGW is the worst at low frequencies with the reversed tendency at high frequencies. For U equal 5 the accuracy of the QPG Γ_E W approach deteriorates also at low frequencies and its failing at higher frequencies becomes severe. The important point here is, that the above high-frequency tendencies in the QP-based methods correlate well with the tendencies in the internal energy as one can easily see. Namely, for $U \leq 1$ the the QPG Γ_E W gives the best (among the QP-based schemes) internal energy and for $U > 1$ it is the worst among them. This also correlates very well with the deviations from the full WI.

For $U=0.5$ the QPGW approach produces the best G at lowest frequencies among all approximate methods. One can speculate, that this fact is similar to the well known fact, that in weakly correlated real materials the QPGW is probably the best approach for studying the spectra (which are defined by the low frequency behavior of Green's function). This fact can be related with the exact fulfillment of the long-wave limit of the WI in the QPGW approach.

An interesting observation comes from the figure for

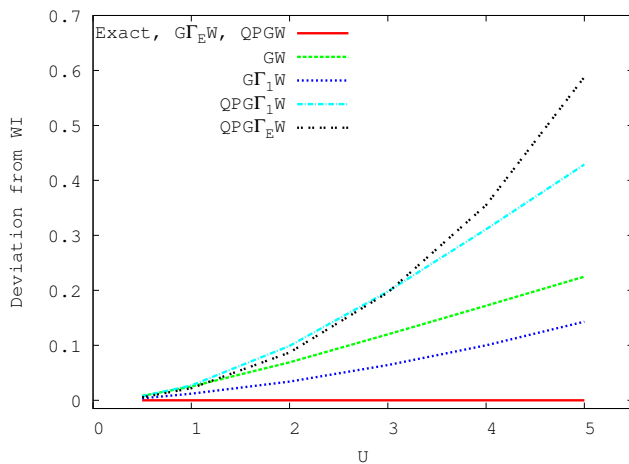


FIG. 10: (Color online) $\mathbf{q} \rightarrow 0$ Ward Identity average violation as a function of U parameter.

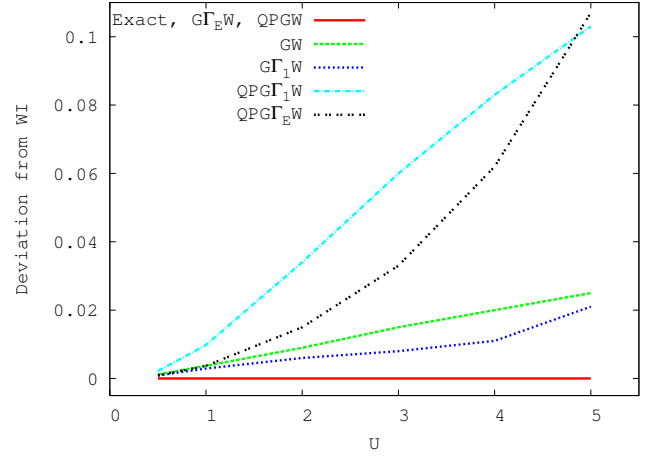


FIG. 11: (Color online) $\mathbf{q} \rightarrow 0, \nu \rightarrow 0$ Ward Identity average violation as a function of U parameter.

$U=1$. As one can see there is a strict separation in the accuracy of G obtained within the QP-group and within the non QP-group. The reasons for this feature have not been studied in this work but it could be related to the above mentioned swapping between different tendencies in the QP-based methods at this U .

The GW-based (without the QP approximation) methods give numerically exact internal energy till $U \approx 2$ which is not very surprising because they are conserving (in Baym-Kadanoff sense¹³) and in the weakly correlated regime should produce accurate total energies. Generally it is not a good idea to use the QP-based methods to evaluate the total energy because even if they originate from the same Ψ -functional¹⁴ as the GW-based methods the Dyson equation (DE) is not satisfied in them anymore. As it was indicated above, the deviations from the exact Green's function in the QP-based approaches are especially noticeable at high frequencies which are important for the total energies evaluation. The results shown in Fig.8 clearly support this point of view.

Internal energy obtained in QP-based approximations deviates significantly from the exact one even at small U . It is interesting that in the QPGW scheme the error remains almost unchanged till $U = 5$ which probably is accidental because at $U \geq 3$ the PT becomes unreliable. The important difference between the GW-based and the QPGW-based methods is however that the $G\Gamma_1W$ improves the internal energy as compared to the GW, whereas applying the vertex of improved accuracy ($1 \rightarrow \Gamma_1 \rightarrow \Gamma_E$) in the sequence $QPGW \rightarrow QPG\Gamma_1W \rightarrow QPG\Gamma_EW$ makes the results worse and worse which also tells us that one should not apply the vertex correction combined with the QP approximation.

As it is clear, the degree of violation of the WI correlates well with the errors in the Green functions at average and high frequencies, which are responsible for the accuracy of the calculated total energies. And indeed,

the comparison of the Figures 8 and 9 tells us, that the accuracy of the total energy and the accuracy of the full WI fulfillment are closely related. Thus, the full WI can be useful as a measure of the accuracy of the calculated total energies.

There was a hope, that the deviation from the long-wave+static limit of the WI correlates well with the errors in G at low frequencies. But for the two-site Hubbard model this seems to be not the case (besides the above mentioned success of the QPGW approach at the smallest values of U). However, in real materials where the spectra obtained with the QPGW are generally noticeably better than the spectra obtained with the scGW the situation might be different.

IV. CONCLUSIONS

In this work the Hedin's equations¹² for the two-site Hubbard model have been solved self-consistently with and without applying the quasiparticle approximation for the Green function. The study has been performed both when the exact three-point vertex function was used as an input and when the perturbative theory (in its zero and first orders in W) was used to evaluate the corresponding vertices self-consistently. The results of this work obtained with the exact vertex have direct impact on what one can expect from the future implementation of the sc GW+DMFT and the sc QPGW+DMFT schemes. As it has been shown here, only the GW+DMFT approach can be considered as useful approximation. However, as it was said in the Introduction, this work deals with an ideal situation, when the GW part and the DMFT part are perfectly separable and the subspace where GW is used is very weakly correlated (so that GW and QPGW give identical results for the weakly correlated subspace). In practice, it is not always the case. The correlations in

the "GW"-subspace might be noticeable. In such situation, the QPGW might be superior (with respect to the GW) for the subspace not included in the DMFT part. The conclusions about the DMFT part obviously remain as before - one should not impose the QP approximation on G in the DMFT part. As it seems, in such circumstances the preference should be given to the approach (GW-based or QPGW-based) depending on which subspace (the "weakly" or the "strongly" correlated) is more important for the problem under consideration. However, on the fundamental level, such a situation should be resolved either by the increasing of the subspace covered by the DMFT part or (which seems to be easier practically) by including more diagrams beyond GW for the "weakly" correlated subspace.

It has been shown, that the methods with the PT-based vertices (when they are applicable) reveal similar tendencies (for example if one chooses between the QP self-consistency and the full sc) as the methods based on the exact vertices. Namely, when the correlation strength increases, both the PT-based and the exact vertices-based schemes begin to fail if one uses the QP self-consistency. Also of practical importance is the finding that the violation of the WI in any particular method correlates well with the general applicability of the given method. This can be an useful information if one sees to apply the schemes with vertex corrections to the real materials where the exact solutions are not available to serve as a judgement.

The results of this work are of the methodological importance. Of course the two-site HM doesn't cover all possible regimes of correlations which may happen in realistic materials. In order to cover a little bit more of the possible regimes of correlations the similar work on the homogeneous electron gas is now being performed (with the three-point vertex functions calculated within the PT only).

¹ P. Sun and G. Kotliar, Phys. Rev.B **66**, 085120 (2002).

² S. Biermann, F. Aryasetiawan, and A. Georges, Phys. Rev. Lett. **90**, 086402 (2003).

³ J. M. Tomczak, M. Casula, T. Miyake, and S. Biermann, Phys. Rev. B **90**, 165138 (2014).

⁴ A. N. Rubtsov, V. V. Savkin, and A. I. Lichtenstein, Phys. Rev. B **72**, 035122 (2005).

⁵ P. Werner, A. Comanac, L. de Medici, M. Troyer, and A. J. Millis, Phys. Rev. Lett. **97**, 076405 (2006).

⁶ A. Kutepov, K. Haule, S. Y. Savrasov, and G. Kotliar, Phys. Rev. B **85**, 155129 (2012).

⁷ A. Kutepov, S. Y. Savrasov, and G. Kotliar, Phys. Rev. B **80**, 041103 (2009).

⁸ T. Kotani and M. van Schilfhaarde, S. V. Faleev, Phys. Rev.B **76**, 165106 (2007).

⁹ M. van Schilfhaarde, T. Kotani, and S. Faleev, Phys. Rev. Lett. **96**, 226402 (2006).

¹⁰ J. M. Tomczak, M. van Schilfhaarde, and G. Kotliar, Phys. Rev. Lett. **109**, 237110 (2012).

¹¹ J. Tomczak, arXiv.cond.mat.:1411.5180 (2014).

¹² L. Hedin, Phys. Rev. **139**, A796 (1965).

¹³ G. Baym, and L. P. Kadanoff, Phys. Rev. **124**, 287 (1961).

¹⁴ C.-O. Almbladh, U. von Barth and R. van Leeuwen, Int. J. of Mod.Phys. B **13**, 535 (1999).